

Derivation of Dynamic Model of Two-Input-Two-Output Torque Difference Amplification Motor Drive System and Independent Left-and-Right Wheel Control with Decoupling Compensator

Hiroyuki Fuse ^{*a)}	Student Member,	Hiroshi Fujimoto*	Senior Member
Kaoru Sawase ^{**}	Non-member,	Naoki Takahashi ^{**}	Non-member
Ryota Takahashi ^{**}	Non-member,	Yutaro Okamura ^{**}	Non-member
Ryosuke Koga ^{**}	Non-member		

A torque vectoring differential (TVD) enhances the cornering performance by generating a torque difference between the left and right wheels. For electrified vehicles, a TVD with a two-motor-torque difference amplification mechanism (TDA-TVD) has been proposed and it generates a greater torque difference compared to an Individual-wheel-drive (IWD) system under the same power output from the traction motors. However, due to the complex gear reduction system including planetary gears and driveshafts, TDA-TVD has problems with the vibration of both the driveshaft torque and the yaw rate while cornering. To deal with these problems, this paper first derives a detailed dynamic model of TDA-TVD. Secondly, a decoupling compensator is designed in order to achieve an independent drive of the left and right wheels so that any motor drive algorithm designed for IWD systems can be applied. Thirdly, a vibration suppression controller is designed. Then, simulations and experimental evaluations using a real vehicle with the TDA-TVD are demonstrated. The experimental results show the effectiveness of the vibration suppression of driveshafts and yaw rate.

Keywords: Electric Vehicle, Motor Drive System, Two-Input-Two-Output System, Vibration Suppression, Decoupling Compensation, Torque Vectoring Differential

1. Introduction

A torque vectoring differential (TVD) is a device that controls direct yaw moment by generating a torque difference between the left and right wheels. TVD has the advantage of improving the cornering performance by actively controlling the yaw moment [1] [2] [3].

For that reason, some electric vehicles adopt individual-wheel-drive (IWD) systems (either with on-board or in wheel motor) and a lot of torque vectoring or distribution algorithms have been studied [4] [5] [6]. However, the maximum available torque difference and direct yaw moment decrease when the vehicle is at high speed, and the same problem occurs when the vehicle is cornering near the critical region, due to the decreased traction of the inner wheels caused by the load transfer.

A TVD with a two-motor-torque difference amplification mechanism (TDA-TVD) has been proposed in order to increase the maximum available torque difference [7] [8]. While TDA-TVD has the same advantages as the TVD, it has relatively complex mechanical components, including plane-

tary gears, reduction gears, and driveshafts. This leads to undesirable vibrations of the driveshaft torque on the wheels and yaw rate vibration while cornering with its torque vectoring system in function. The previous study [7] [8] did not derive the dynamic model of TDA-TVD that describes its anticipated vibrations of the driveshaft torque and yaw motion. These problems limit the performance of TDA-TVD and must be solved in order to achieve its full potential.

Vibration suppression in vehicles has been widely studied for a long time because they have a lot of vibrating components such as internal combustion engines, transmissions, driveshafts, and tires. In the case of EVs, even though their driveline tends to be simpler than internal combustion engine vehicles (ICVs), the relatively fast torque response of electric motors can create uncomfortable shaking vibration originating from the driveshafts when referring to on-board EVs. In order to deal with these problems, various anti-jerk controllers have been studied and proposed [9] [10] [11]. Each study basically constructs a certain dynamic model of the driveline of the target EVs and implements either or both a feedback and a feedforward controller. A majority of these studies consider EVs with a single-input-single-output drive system (e.g., a single on-board motor drives the two front or rear wheels, or single on-board or in-wheel motor drives the left or right wheel individually). Therefore, these studies cannot be directly applied to TDA-TVD due to the difference in the mechanical structure.

a) Correspondence to: fuse.hiroyuki17@ae.k.u-tokyo.ac.jp

* The University of Tokyo
7H1, Transdisciplinary Sciences Bldg.,5-1-5, Kashiwanoha,
Kashiwa, Chiba, Japan, 277-8561

** MITSUBISHI MOTORS CORPORATION
1, Nakashinkiri, Hashimecho, Okazaki, Aichi, Japan, 444-8501

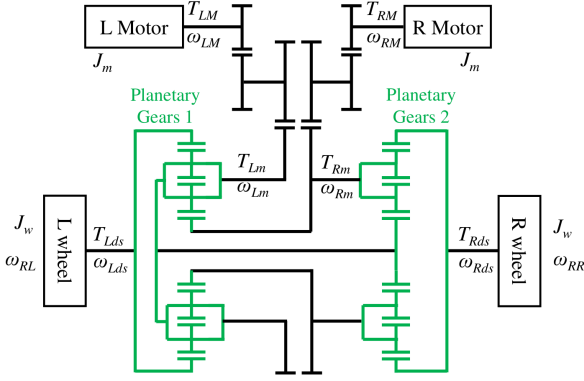


Figure 1: Schematic diagram of TDA-TVD [8].

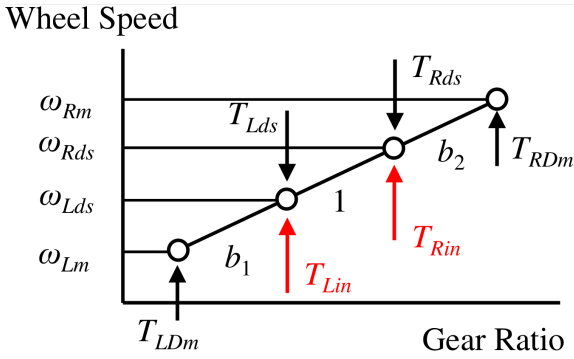


Figure 2: Velocity diagram of TDA-TVD.

First, this study constructs a detailed dynamic model of TDA-TVD to describe the mechanical coupling of its drive system between the left and right wheels. Next, this study designs a decoupling compensator that enables us to control the left and right wheels independently, based on the obtained dynamic model of TDA-TVD. With the decoupling compensator, we can apply conventional vibration suppression controls originally designed for IWD systems. This way, we can treat TDA-TVD as an IWD system and the overall vehicle dynamics control system will be significantly simpler.

As a demonstration of the validity of the obtained dynamic model of TDA-TVD and decoupling compensator, a simple feedforward vibration suppression controller based on the inverse model of the decoupled drive system is designed, simulated, and experimentally tested.

2. Derivation of the dynamic model of TDA-TVD

Several types of TDA-TVD have been proposed by Sawase [7] [8]. As an example of those, a schematic diagram of TDA-TVD is shown in Fig. 1. Regardless of the different types of TDA-TVD, the following equations can be derived comprehensively. The motor torques T_{RM} and T_{LM} are amplified by the primary gear ratio G through the primary reduction gears and become T_{RDm} and T_{LDm} , respectively. After passing through the following planetary gears, the driveshaft torques T_{Rds} and T_{Lds} are transmitted to the wheels. The relation of the rotation speed and torque is visually represented by a velocity diagram as shown in Fig. 2 [8]. In the figure, b_1 and b_2 are the equivalent secondary reduction gear ratios determined by each gear of the planetary gears. b_1 and b_2 are designed to be almost equal. From Fig. 2, we have the

following equations

$$T_{Rin} = (b_2 + 1)T_{RDm} - b_1T_{LDm} \dots\dots\dots(1)$$

$$T_{Lin} = (b_1 + 1)T_{LDm} - b_2T_{RDm} \dots\dots\dots(2)$$

where T_{Rin} and T_{Lin} are the input motor torque imaginarily converted to the driveshaft side. T_{Rin} and T_{Lin} are convenient to deal with the mechanical coupling which will be explained later. T_{Rm} and T_{Lm} in Fig. 1 are the transmitted motor torques to the planetary gears after the gear reduction and represented by

$$T_{Rm} = T_{RDm} - T_{RIm} \dots\dots\dots(3)$$

$$T_{Lm} = T_{LDm} - T_{LI m} \dots\dots\dots(4)$$

$$T_{RIm} = G^2 J_m \dot{\omega}_{Rm} \dots\dots\dots(5)$$

$$T_{LI m} = G^2 J_m \dot{\omega}_{Lm} \dots\dots\dots(6)$$

where T_{RIm} and $T_{LI m}$ are inertia torques of the motor, J_m is the inertia of the motor, and ω_{Rm} and ω_{Lm} are the motor side angular speeds after the primary gear reduction. ω_{Rm} , ω_{Lm} and the driveshaft side angular speeds ω_{Rds} and ω_{Lds} have the following relations

$$\omega_{Rm} = (b_2 + 1)\omega_{Rds} - b_2\omega_{Lds} \dots\dots\dots(7)$$

$$\omega_{Lm} = -b_1\omega_{Lds} + (b_1 + 1)\omega_{Rds} \dots\dots\dots(8)$$

2.1 Derivation of the linearized model

This section derives the linearized model of TDA-TVD. From the equations of TDA-TVD shown earlier, we can derive the following equations using matrices and vectors

$$J\dot{\omega}_{ds} = T_{in} - T_{ds} \dots\dots\dots(9)$$

where

$$J = \begin{pmatrix} J_{11} & J_{12} \\ J_{21} & J_{22} \end{pmatrix} \dots\dots\dots(10)$$

$$J_{11} = [(b_2 + 1)^2 + b_1^2]G^2 J_m \dots\dots\dots(11)$$

$$J_{12} = J_{21} = -[b_1(b_1 + 1) + b_2(b_2 + 1)]G^2 J_m \dots\dots(12)$$

$$J_{22} = [(b_1 + 1)^2 + b_2^2]G^2 J_m \dots\dots\dots(13)$$

$$\dot{\omega}_{ds} = \begin{pmatrix} \dot{\omega}_{Rds} \\ \dot{\omega}_{Lds} \end{pmatrix} \dots\dots\dots(14)$$

$$T_{in} = \begin{pmatrix} T_{Rin} \\ T_{Lin} \end{pmatrix} = K T_m \dots\dots\dots(15)$$

$$K = \begin{pmatrix} k_{11} & k_{12} \\ k_{21} & k_{22} \end{pmatrix} = \begin{pmatrix} b_2 + 1 & -b_1 \\ -b_2 & b_1 + 1 \end{pmatrix} \dots\dots\dots(16)$$

$$T_m = \begin{pmatrix} T_{RDm} \\ T_{LDm} \end{pmatrix} \dots\dots\dots(17)$$

$$T_{ds} = \begin{pmatrix} T_{Rds} \\ T_{Lds} \end{pmatrix} \dots\dots\dots(18)$$

In this paper, we assume that all the elasticity and viscosity of TDA-TVD are equivalently represented by the driveshaft stiffness K_s and damping factor D_s . With this assumption, the driveshaft torque T_{jds} (subscript j is either l (left) or r (right)) and the driveshaft angular speed ω_{jds} have the following relations [11] [12]

$$T_{jds} = \left(\frac{K_s}{s} + D_s \right) (\omega_{jds} - \omega_{Rj}) \dots\dots\dots(19)$$

$$\omega_{Rj} = \frac{T_{jds}}{J_{all}s} \dots \dots \dots (20)$$

$$J_{all} = J_w + r^2 M(1 - \lambda_n)/2, \dots \dots \dots (21)$$

where ω_{Rj} is the angular speed of the rear wheel, J_{all} is the nominal inertia of the wheel at the nominal slip ratio λ_n (0: when the wheel is not slipping, 1: when the wheel is slipping), r is the effective radius of the wheel, and M is the vehicle mass. Assuming that the wheel rotates at the nominal slip ratio λ_n , the nonlinear dynamics between the wheel and the road can be linearized. From (19) and (20), we get the following equation

$$\dot{\omega}_{ds} = \frac{J_{all}s^2 + D_s s + K_s}{J_{all}(D_s s + K_s)} T_{ds} \dots \dots \dots (22)$$

By substituting (22) to (9), we have

$$\left(E_2 + \frac{J_{all}s^2 + D_s s + K_s}{J_{all}(D_s s + K_s)} J \right) T_{ds} = T_{in} \dots \dots \dots (23)$$

where E_2 is an identity matrix of size 2. Here, we define a matrix g given by

$$g = \begin{pmatrix} g_{11} & g_{12} \\ g_{21} & g_{22} \end{pmatrix} = \left(E_2 + \frac{J_{all}s^2 + D_s s + K_s}{J_{all}(D_s s + K_s)} J \right)^{-1} \dots (24)$$

Now we have

$$T_{ds} = g T_{in} \dots \dots \dots (25)$$

$$\begin{pmatrix} T_{Rds} \\ T_{Lds} \end{pmatrix} = \begin{pmatrix} g_{11} & g_{12} \\ g_{21} & g_{22} \end{pmatrix} \begin{pmatrix} T_{Rin} \\ T_{Lin} \end{pmatrix} \dots \dots \dots (26)$$

From the above equation, we can derive the four transfer functions as follows

$$\frac{T_{Rds}}{T_{Rin}} = g_{11} = \frac{g_{11n}}{g_d} \dots \dots \dots (27)$$

$$\frac{T_{Rds}}{T_{Lin}} = g_{12} = \frac{g_{12n}}{g_d} = \frac{T_{Lds}}{T_{Rin}} = g_{21} \dots \dots \dots (28)$$

$$\frac{T_{Lds}}{T_{Lin}} = g_{22} = \frac{g_{22n}}{g_d} \dots \dots \dots (29)$$

$$g_{11n} = J_{all} \{ J_{22} J_{all} s^3 + ((J_{22} + J_{all}) D_s^2 + J_{22} J_{all} K_s) s^2 + 2K_s D_s (J_{22} + J_{all}) s + K_s^2 (J_{22} + J_{all}) \} \dots (30)$$

$$g_{12n} = g_{21n} = -J_{12} J_{all} (J_{all} D_s s^3 + (J_{all} K_s + D_s^2) s^2 + 2K_s D_s s + K_s^2) \dots (31)$$

$$g_{22n} = J_{all} \{ J_{11} J_{all} s^3 + ((J_{11} + J_{all}) D_s^2 + J_{11} J_{all} K_s) s^2 + 2K_s D_s (J_{11} + J_{all}) s + K_s^2 (J_{11} + J_{all}) \} \dots (32)$$

$$g_d = |J| J_{all}^2 s^4 + J_{all} D_s (2|J| + (J_{11} + J_{22}) J_{all}) s^3 + (|J| (2J_{all} K_s + D_s^2) + J_{all} (J_{11} + J_{22}) (D_s^2 + J_{all} K_s) + J_{all}^2 D_s^2) s^2 + 2K_s D_s (|J| + (J_{11} + J_{22}) J_{all} + J_{all}^2) s + K_s^2 (|J| + (J_{11} + J_{22}) J_{all} + J_{all}^2) \dots (33)$$

$$|J| = J_{11} J_{22} - J_{12} J_{21} = G^4 J_m^2 (b_1 + b_2 + 1)^2 \dots (34)$$

Now we have obtained the linear model of TDA-TVD. The block diagram of TDA-TVD is represented in Fig. 3. In the figure, the following relations are given to represent the parameters.

$$J^{-1} = \frac{1}{|J|} \begin{pmatrix} J_{22} & -J_{12} \\ -J_{21} & J_{11} \end{pmatrix} = \begin{pmatrix} h_{11} & h_{12} \\ h_{21} & h_{22} \end{pmatrix} \dots \dots \dots (35)$$

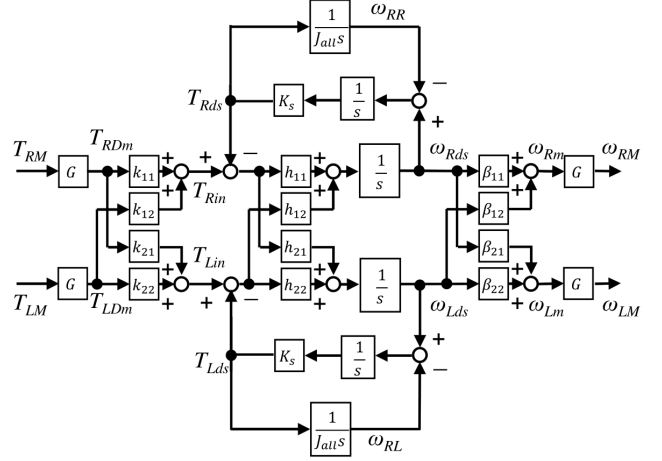


Figure 3: Block diagram of TDA-TVD.

$$\begin{pmatrix} \omega_{Rm} \\ \omega_{Lm} \end{pmatrix} = \begin{pmatrix} b_2 + 1 & -b_2 \\ -b_1 & b_1 + 1 \end{pmatrix} \begin{pmatrix} \omega_{Rds} \\ \omega_{Lds} \end{pmatrix} \dots \dots \dots (36)$$

$$= \begin{pmatrix} \beta_{11} & \beta_{12} \\ \beta_{21} & \beta_{22} \end{pmatrix} \begin{pmatrix} \omega_{Rds} \\ \omega_{Lds} \end{pmatrix} = B \begin{pmatrix} \omega_{Rds} \\ \omega_{Lds} \end{pmatrix}$$

3. Design of the joint torque controller for TDA-TVD

This section derives and designs a joint torque controller (JTC) for TDA-TVD that suppresses the driveshaft torque vibration. The JTC is composed of a driveshaft-motor torque converter, a decoupling compensator, and a feedforward controller.

3.1 Design of the driveshaft-motor torque converter

TDA-TVD has the two inputs T_{RM} and T_{LM} which we can freely control, and two outputs ω_{RM} and ω_{LM} as the obtainable values through the drive-side angular speed sensor which are used to drive the electric motors.

In order to control the converted motor-side torque inputs T_{Rin} and T_{Lin} and estimate the driveshaft angular speeds ω_{Rds} and ω_{Lds} , we can utilize the following relations from (15), (16), and (37)

$$\begin{pmatrix} \omega_{Rds-est} \\ \omega_{Lds-est} \end{pmatrix} = G^{-1} B^{-1} \begin{pmatrix} \omega_{RM} \\ \omega_{LM} \end{pmatrix} \dots \dots \dots (37)$$

$$\begin{pmatrix} T_{RM} \\ T_{LM} \end{pmatrix} = G^{-1} K^{-1} \begin{pmatrix} T_{Rin-ref} \\ T_{Lin-ref} \end{pmatrix} \dots \dots \dots (38)$$

The first equation is called ‘‘driveshaft angular speed estimator’’ (DSE) and the second equation is called ‘‘driveshaft-motor torque converter’’ (DMTC).

With this DMTC, the driveshaft torque can be controlled, but with slight errors due to the inertia torque of the motors and the coupling. Some sort of wheel speed control or anti-skid-wheel control can be implemented and achieved with the DMTC. However, as mentioned earlier, due to the elasticity and viscosity of TDA-TVD, an undesirable vibration is inevitable. The DMTC will be also called a base controller in the later simulations and experiments.

3.2 Design of the decoupling compensator

In order to directly control the driveshaft torque itself, we need to construct a decoupling compensator so that the left and right wheels can be independently controlled. The decou-

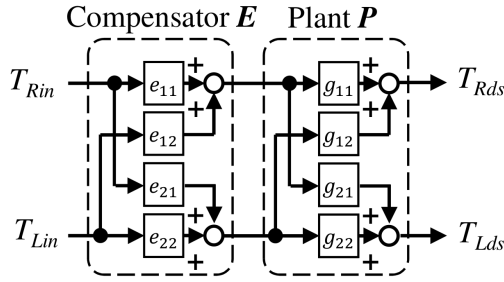


Figure 4: Decoupling compensator E is inserted before TDA-TVD (Plant P).

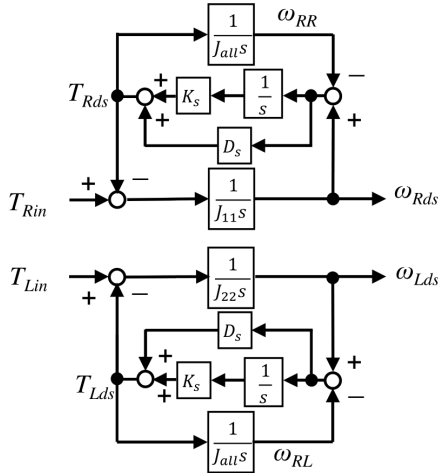


Figure 5: Equivalent block diagram of TDA-TVD with decoupling compensator E .

plung compensator E is added before the direct torque controller, as shown in Fig. 4. In the figure, the plant P is the TDA-TVD with the DMTC. but the outputs are the driveshaft torques. Thankfully, there is a traditional method called “diagonalization” of multi-input-multi-output systems [13] and each gain of the decoupling compensator E is given by

$$e_{11} = e_{22} = 1 \dots \dots \dots (39)$$

$$e_{12} = -\frac{g_{12}}{g_{11}} = -\frac{g_{12n}}{g_{11n}} \dots \dots \dots (40)$$

$$e_{21} = -\frac{g_{21}}{g_{22}} = -\frac{g_{12n}}{g_{22n}} \dots \dots \dots (41)$$

Now, the transfer functions with the decoupling compensator E are obtained as follows

$$\frac{T_{Rds}}{T_{Rin}} = \frac{J_{all}(D_s s + K_s)}{J_{11} J_{all} s^2 + D_s (J_{11} + J_{all}) s + K_s (J_{11} + J_{all})} \dots (42)$$

$$\frac{T_{Rds}}{T_{Lin}} = \frac{T_{Lds}}{T_{Rin}} = 0 \dots \dots \dots (43)$$

$$\frac{T_{Lds}}{T_{Lin}} = \frac{J_{all}(D_s s + K_s)}{J_{22} J_{all} s^2 + D_s (J_{22} + J_{all}) s + K_s (J_{22} + J_{all})} \dots (44)$$

The equivalent block diagram of TDA-TVD with the decoupling compensator E is shown in Fig. 5. It clearly suggests that the left and right wheels can be controlled independently.

The transfer functions of the decoupled system have second order characteristic polynomials. The decoupled system

has a pair of conjugate complex roots $-\alpha \pm j\beta$ ($j = \sqrt{-1}$) given by

$$\alpha = \frac{D_s (J_M + J_{all})}{2 J_M J_{all}} \dots \dots \dots (45)$$

$$\beta = \frac{1}{2} \sqrt{\frac{J_M + J_{all}}{J_M J_{all}} \left(4 K_s - \frac{D_s (J_M + J_{all})}{J_M J_{all}} \right)} \dots \dots \dots (46)$$

where J_M is either J_{11} or J_{22} . The step response of the decoupled system ($T_{jin}(t) = 1$) is given by

$$T_{jds}(t) = \frac{J_{all}}{J_M + J_{all}} (1 - e^{-\alpha t} \cos \beta t) + \frac{D_s}{2 J_M \beta} e^{-\alpha t} \sin \beta t$$

$$\approx \frac{J_{all}}{J_M + J_{all}} (1 - e^{-\alpha t} \cos \beta t) \dots \dots \dots (47)$$

The equation suggests that the final value will have a slight error due to the motor side inertia. With the typical parameters as shown in Tab. 1, we can assume $J_M \ll J_{all}$ and $4 J_M K_s \gg D_s$ and we can derive $\frac{J_{all}}{J_M + J_{all}} \approx 1$ and $\frac{D_s}{2 J_M \beta} \approx \frac{D_s}{2 \sqrt{J_M K_s}} < \frac{1}{10}$. Therefore, the second term of the right side of this equation is negligible compared to the first term. The normalized overshoot of the step response of the decoupled system OS is obtained by substituting $t = \pi/\beta$ to (47) as follows

$$OS = e^{-\alpha \pi / \beta} \dots \dots \dots (48)$$

As an example, a vehicle with typical parameters as shown in Tab. 1 has a driveshaft vibration frequency of $\beta/(2\pi) = 2.922$ Hz, and the normalized overshoot $OS = 0.749$ ($J_M = J_{11}$). This causes undesirable driveshaft and yaw rate vibrations that must be suppressed.

3.3 Design of the feedforward controller A feedforward controller is designed by the inverse of the transfer function of the decoupled system $\frac{T_{jin}}{T_{jds}}$ [12], which is given by

$$C_{FF} = \frac{J_M J_{all} s^2 + D_s (J_M + J_{all}) s + K_s (J_M + J_{all})}{J_{all} (D_s s + K_s)} \dots (49)$$

Since C_{FF} is not proper, a low pass filter (LPF) Q_{FF} is added. With this feedforward controller, the decoupling compensator and the DMTC, the transfer function $\frac{T_{jds}}{T_{jds-ref}}$ becomes a unity (i.e., 1) so that undesirable vibration could be suppressed.

A feedback controller can also be designed and implemented in the same way with [12]. However, in order to evaluate the derived dynamic model and the decoupling compensator of TDA-TVD, this study only implements the feedforward controller for the simulations and experiments.

4. Simulations of the joint torque controller for TDA-TVD

Simulations of the JTC for TDA-TVD is conducted using MATLAB and Simulink environment. The wheel model is approximated by a linear model as shown in Fig. 3.

4.1 Simulation conditions In order to evaluate the performance of the JTC, the base controller without the JTC, the JTC with the feedforward and the decoupling compensator are tested. The left and right wheels are driven with independently different reference torque values for three seconds. In each case, the vehicle accelerates from a stand still

Table 1: Simulated vehicle parameters.

Vehicle mass M	1500 kg
Effective wheel radius r	0.35 m
Wheel inertia J_ω	1.5 kg·m ²
Motor inertia J_m	0.02 kg·m ²
Primary reduction gear ratio G	12
Equivalent secondary reduction gear ratio b_1, b_2	0.7, 0.71
Stiffness of driveshaft K_s	3000 N/rad
Damping factor of driveshaft D_s	30 N/(rad/s)
Nominal slip ratio λ_n	0
Nominal wheel inertia J_{all}	93.38 kg·m ²
Inertia matrix J_{11}, J_{12}, J_{22}	9.83, -6.92, 9.77 kg·m ²
Step response parameters α, β, OS ($J_M = J_{11}$)	1.686, 18.36, 0.749

Table 2: Parameters of joint torque controller.

Left side driveshaft torque reference $T_{Lds-ref}$	-450 Nm
Right side driveshaft torque reference $T_{Rds-ref}$	450 Nm
Rate limiter for $T_{jds-ref}$	± 2000 Nm/s
Cutoff frequency of Q_{FF}	10 Hz

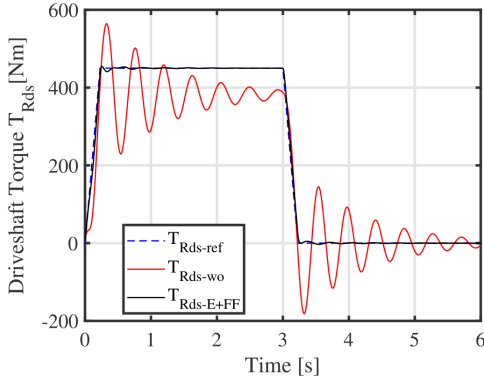


Figure 6: Simulation result of driveshaft torque response.

condition. The reference driveshaft torque $T_{jds-ref}$ changes in a “step manner” with a rate limiter of 2000 N/s. Tab. 1 and Tab. 2 show the specification of the simulated vehicle and parameters of the JTC.

4.2 Simulation results Fig. 6 shows the simulation results of the driveshaft torque T_{Rds} response. In the figures, subscription ref, wo, and E+FF suggest the reference value of the driveshaft torque (blue dashed line), measured value with the base control (red line) and with full JTC (black line), respectively. Obviously, the base control (without the JTC, red line) has the largest vibration and overshoot of all cases. In addition, since the base control does not consider the motor inertia torque at all, a certain offset error remains. The magnitude and degree of the offset error depend on the torque difference between the left and right wheels. The wheel which has the largest torque input always has a smaller driveshaft torque value compared to the reference value, and vice versa.

On the other hand, the full JTC reduces the joint torque vibration significantly. Furthermore, during the transition, driveshaft torques follow the reference values almost without delay.

5. Experimental validations of the joint torque controller for TDA-TVD

Experimental validation of the JTC for TDA-TVD is conducted using a real vehicle with the TDA-TVD unit. The experimental vehicle is shown in Fig. 7. The experimental



Figure 7: Experimental vehicle equipped with TDA-TVD.

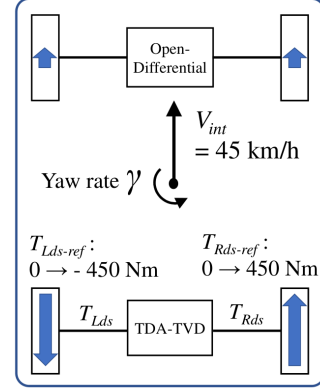


Figure 8: Illustration of the experiment.

Table 3: Evaluation of joint torque controller.

	Without JTC	JTC
Offset error $e_{T_{Rds}}$ [%]	-14.1	-5.4
Overshoot $OS_{T_{Rds}}$ [%]	69.8	18.2
Settling time $t_{s-T_{Rds}}$ [s]	1.19	0.80
Overshoot OS_γ [%]	100.0	23.4
Settling time $t_{s-\gamma}$ [s]	1.21	1.23

vehicle is equipped with a device that can measure driveshaft torques T_{jds} on both sides.

5.1 Experimental conditions Fig. 8 illustrates the experimental verification. The experimental vehicle goes on a straight path at a speed of 45 km/h driven by the front wheels. Then, the rear wheels are driven with a torque difference of 900 Nm for 3 seconds, which is the same condition with the simulation shown earlier. While the torque vectoring system is working, the steering angle is maintained at 0 degree by the driver.

The JTC is implemented with the vehicle parameters of the experimental vehicle. The equivalent stiffness and damping factor of the driveshaft (K_s and D_s) of the experimental vehicle were estimated by measuring the driveshaft torque of the step response. Correspondingly with the simulation, both sides of the driveshaft torque T_{jds} are measured and their responses are evaluated with two situations: without the JTC and with the full JTC. Yaw rate γ is also measured and evaluated.

5.2 Experimental results Fig. 9 shows the experimental results of the JTC for TDA-TVD. There are large vibrations of the measured driveshaft torques T_{jds} and yaw rate γ with the base control (without the JTC), in addition to the non-negligible offset error. On the other hand, both vibrations are considerably reduced with the JTC. Overshoots

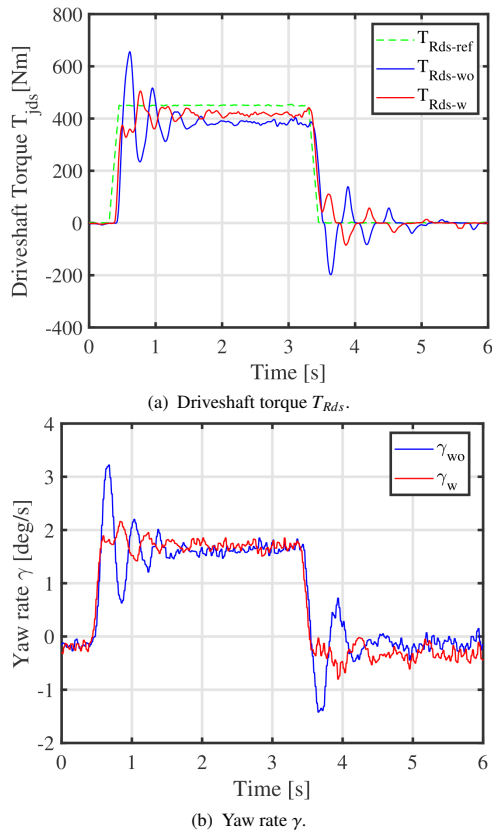


Figure 9: Experimental results with JTC.

of driveshaft torques T_{Rds} and yaw rate γ become about one third and one fourth, respectively. Furthermore, the rise of the driveshaft torques T_{jds} becomes rather slightly sharper, without compromising the response.

Tab. 3 quantitatively shows the performance of each of the controllers. On the table, e_{TRds} is the offset error of the right side driveshaft torque T_{Rds} between the settling value and the reference value. Overshoot OS_{TRds} is the difference between the value of the first peak and the settling value of the right side driveshaft torque T_{Rds} . Settling time t_{s-TRds} is the duration between the moment T_{Rds} settles within $\pm 5\%$ of the settling value. Overshoot OS_γ and settling time $t_{s-\gamma}$ are defined in the same way.

Overall experimental results confirm the validity of the derived dynamic model of TDA-TVD, the effectiveness of the decoupling compensator and the feedforward controller. However, offset errors still remain likely due to the unmodeled/neglected elements such as the coupling cause by a certain viscosity between the left and right wheels (i.e. planetary gears), and the inertia of gears. Better tracking and control of the driveshaft torque T_{jds} could be achieved by more a detailed system identification including the aforementioned elements and its investigation will be future work. Furthermore, co-use of the feedback controller and various conventionally proposed vibration suppression algorithms could improve the performance as well and will also be investigated in the future.

6. Conclusion

This study proposed a dynamic model and a decoupling compensator of a two-input-two-output torque vectoring dif-

ferential with torque difference amplification (TDA-TVD) for electrified vehicles in order to achieve both independent drive of the left and right wheels and improved controllability. The decoupled system of TDA-TVD can be treated as an Individual-wheel-drive (IWD) system and any conventional vehicle dynamics and motor drive controllers for IWD system can be applied. As a benchmark, a feedforward-based vibration suppression controller was applied and tested. The results of experimental evaluations using a real vehicle with a TDA-TVD unit showed that both the driveshaft torque and yaw rate vibrations were reduced to about 25% compared to the baseline without any control while the torque vectoring is in function. The process of modeling of any two-input-two-output motor drive systems and designing of its controllers will be significantly more efficient with the proposed approach. An improved and more detailed system identification of TDA-TVD such as the viscosity coupling, implementation of an additional feedback controller, and further improvement of the vibration reduction will be future work.

References

- (1) Y. Shibahata, K. Shimada, and T. Tomari, "Improvement of vehicle maneuverability by direct yaw moment control," *Veh. Syst. Dyn.*, vol. 22, no. 5-6, pp. 465-481, 1993.
- (2) K. Sawase, Y. Ushiroda, and T. Miura, "Left-right torque vectoring technology as the core of super all wheel control (S-AWC)," *Mitsubishi Motors Tech. Rev.*, vol. 18, pp. 16-23, 2006.
- (3) L. Zhang, H. Ding, Y. Huang, H. Chen, K. Guo and Q. Li, "An Analytical Approach to Improve Vehicle Maneuverability via Torque Vectoring Control: Theoretical Study and Experimental Validation," *IEEE Trans. on Vehicular Technology*, vol. 68, no. 5, pp. 4514-4526, May 2019.
- (4) Y. Hori, "Future vehicle driven by electricity and control research on four-wheel-motored 'UOT electric march II'," *IEEE Trans. on Industrial Electronics*, 51, 5, pp. 954-962, 2004.
- (5) Y. Chen, S. Chen, Y. Zhao, Z. Gao and C. Li, "Optimized Handling Stability Control Strategy for a Four In-Wheel Motor Independent-Drive Electric Vehicle," in *IEEE Access*, vol. 7, pp. 17017-17032, 2019.
- (6) M. Chae, Y. Hyun, K. Yi and K. Nam, "Dynamic Handling Characteristics Control of an in-Wheel-Motor Driven Electric Vehicle Based on Multiple Sliding Mode Control Approach," in *IEEE Access*, vol. 7, pp. 132448-132458, 2019.
- (7) Sawase, K., Chiba M., "Study of Lateral Torque-vectoring Differential Suitable for Electric Powered Vehicles," *Transactions of Society of Automotive Engineers of Japan*, Vol.45-5, p.823-828, 2014 (In Japanese).
- (8) Sawase, K. et al., "Classification and Analysis of Torque-vectoring Differentials with Torque Difference Amplification Mechanism," *Transactions of Society of Automotive Engineers of Japan*, Vol.48, No.2, p.317-322, 2017 (In Japanese).
- (9) H. Kawamura, K. Ito, T. Karikomi, and T. Kume, "Highly-Responsive Acceleration Control for the Nissan LEAF Electric Vehicle," *SAE Technical Paper* 2011-01-0397, 2011.
- (10) A. Scamarcio, M. Metzler, P. Gruber, S. De Pinto and A. Sorniotti, "Comparison of Anti-Jerk Controllers for Electric Vehicles With On-Board Motors," *IEEE Transactions on Vehicular Technology*, vol. 69, no. 10, pp. 10681-10699, Oct. 2020.
- (11) H. Sumiya and H. Fujimoto, "Driving Force Control Method Using Suppression Control of Driving-shaft Vibration for Electric Vehicle with On-board Motor," in *Proc. IEJ Industry Applications Society Conf*, no. 106, 2012, pp. 115-120 (in Japanese).
- (12) S. Wakui, T. Emmei, H. Fujimoto, Y. Hori, "Gear Collision Reduction of Geared In-wheel-motor by Effective Use of Load-side Encoder," *The 45th Annual Conference of the IEEE Industrial Electronics Society*, Lisbon, Portugal, pp.3469-3474, 2019.
- (13) W. Ohnishi, et al., "Decoupling Control Method for High-Precision Stages using Multiple Actuators considering the Misalignment among the Actuation Point, Center of Gravity, and Center of Rotation," *IEEJ Journal of Industry Applications*, Vol.5, No.2, pp.141-147, 2016.